Chloroform Hydrodechlorination Behavior of Alumina-supported Pd and PdAu Catalysts

Juan C. Velázquez and Sukit Leekumjorn
Dept. of Chemical and Biomolecular Engineering, Rice University, 6100 Main Street, Houston, TX 77005

Quang X. Nguyen
Dept. of Electrical and Computer Engineering, Rice University, 6100 Main Street, Houston, TX 77005-1892

Yu-Lun Fang and Kimberly N. Heck
Dept. of Chemical and Biomolecular Engineering, Rice University, 6100 Main Street, Houston, TX 77005

Gary D. Hopkins and Martin Reinhard
Dept. of Civil and Environmental Engineering, Stanford University, Stanford, CA 94305

Michael S. Wong
Dept. of Chemical and Biomolecular Engineering, Rice University, 6100 Main Street, Houston, TX 77005

Dept. of Chemistry, Rice University, 6100 Main Street, Houston, TX 77005

Dept. of Civil and Environmental Engineering, Rice University, 6100 Main Street, Houston, TX 77005

DOI 10.1002/aic.14250
Published online October 31, 2013 in Wiley Online Library (wileyonlinelibrary.com)

Significance

Chloroform is a common groundwater contaminant that is very difficult to remove. Chemically converting it into a less toxic form through heterogeneous catalysis is an attractive approach over conventional physical removal methods if it can be done economically. In this study, we explore the efficacy of supported precious metal catalysts for chloroform hydrodechlorination. We find that Pd/Al_2O_3 is catalytically active for this reaction (6.4 L/g_{Pd}/min) at room temperature, atmospheric pressure, in buffered water, and in the presence of hydrogen gas, and that Pd deposited on commercial Au/Al_2O_3 shows activities as high as 22.4 L/g_{Pd}/min, suggestive of some Pd metal located on top of Au domains. The primary reaction product is methane, with selectivity values exceeding 90%. Surface-enhanced Raman spectroscopy shows evidence of chloroform adsorption and dechlorination on the catalyst surface under aqueous conditions. The results highlight the potential of ambient-condition reductive catalysis to remove chloroform from water. © 2013 American Institute of Chemical Engineers *AIChE J*, 59: 4474–4482, 2013

Keywords: catalysis, environmental engineering, nanoparticles, hydrodechlorination, water

Introduction

Found in at least 717 of the 1430 current or former National Priority List (NPL) sites, the groundwater contaminant of chloroform (CF) is ranked 11th on the Comprehensive Environmental Response, Compensation, and Liability Act (CERCLA) List, based on frequency of occurrence, potential for human exposure, and toxicity.[1,2] The Dept. of Health and Human Services (DHHS), International Agency for Research on Cancer (IARC) and the Environmental Protection Agency (EPA) consider CF a probable human carcinogen associated with colon, urinary bladder, liver and kidney cancers.[3,4] CF belongs to the trihalomethane family, which can be formed from chlorine reacting with naturally occurring organic matter during the water disinfection process.[5] The EPA maximum contaminant limit (MCL) for trihalomethanes in drinking water is 80 μg/L; there is no MCL value for CF.

Industrial spills, leaks and emissions are the principal sources of CF environmental contamination.[3] CF is relatively water-soluble (7.43×10^3 mg/L), with a high-vapor pressure

Additional Supporting Information may be found in the online version of this article.

Correspondence concerning this article should be addressed to M. S. Wong at mswong@rice.edu.

at 293 K (21278 Pa)[6,7] and a relatively low Henry's law constant (312081 atm-L/mol).[8] It hydrolyzes very slowly in water (half-life = 1,850 years at pH = 7).[9] Large quantities of CF are released into the atmosphere and are washed out by rain, thereby entering soil and water bodies. In the atmosphere, CF has a half-life of approximately 80 days, resulting from its reaction with hydroxyl radicals in the stratosphere to produce mostly carbon dioxide and water, and small amounts of phosgene and hydrogen chloride.[10–12] In groundwater, CF contaminant plumes are large,[13] due to its low soil organic carbon sorption coefficient ($K_{oc} = 45$ or log $K_{oc} = 1.65$)[14] and slow hydrolysis rate.

Several *in situ* and *ex situ* technologies have been successfully implemented at CF-contaminated sites. *Ex situ* technologies include soil vapor extraction,[15,16] vacuum-enhanced low temperature thermal desorption,[17] hydraulic containment,[18] activated carbon adsorption,[19] and air stripping.[20] The main disadvantages of *ex situ* technologies are the energy cost associated with pumping water from the subsurface and the formation of a secondary waste stream containing CF, which requires a subsequent treatment step. *In situ* technologies include phytoremediation,[21] permeable reactive barriers,[22] soil capping,[23] monitored natural attenuation,[24] and bioremediation.[25] The most common disadvantage of the *in situ* technologies is the slow rates of CF decrease.

Precious metal catalysis has been studied for CF degradation through gas-phase reductive dechlorination to a limited extent.[26–28] Curiously, this chemistry was explored decades ago to produce dichloromethane (DCM) using an alumina-supported platinum catalyst at moderate temperatures (~473 K),[29] even though DCM is a water contaminant (86th on the CERCLA list).[30]

Matheson and Tratnyek studied the water-phase reductive dehalogenation of chlorinated methanes by iron metal (zero valent iron, ZVI), finding that CF degraded to DCM.[31] Ollis and coworkers studied the water-phase (~313 K) photocatalytic degradation of chloroform over TiO_2, with CO_2 and HCl as the main products.[32,33]

Alvarez and coworkers demonstrated that a microbial-ZVI system provides faster transformation (CF half-life ~1 day) than a ZVI-only system (half-life ~7 days), yielding DCM as main product.[34] They showed that iron corrosion led to the formation of hydrogen, which was then used by anaerobic bacteria as an electron donor for CF dechlorination. Further improvement of ZVI technology was achieved by adding Pd metal to ZVI nanoparticles (particle size ~80–100 nm), which resulted in higher CF degradation rates (CF half-life ~30 min) and decreased DCM formation (up to ~70% of degradation products was methane).[35–37]

Supported Pd catalysts like Pd-on-alumina (Pd/Al_2O_3) are an effective material for the ambient-pressure, room-temperature hydrodechlorination (HDC) of many organochloride compounds dissolved in water.[36,38–48] We previously showed that Pd metal supported on gold nanoparticles (Pd-on-Au NPs) were much more active than Pd-only catalysts.[49–51] These NPs exhibit a clear catalytic activity volcano dependence on Pd surface coverage (or equivalently, Pd content) for trichloroethene and perchloroethene HDC reactions.[52,53] Recent calculations indicate that the Pd-on-Au catalysts are less expensive than Pd-only catalysts,[54] and that the metal catalysis approach is no more expensive than granulated activated carbon adsorption, air-stripping, or permeable reactive barrier technologies.[55]

In this work, we explored Pd/Al_2O_3 and $Pd/Au/Al_2O_3$ of several compositions for room-temperature CF HDC in water. We analyzed their reaction rate constants through batch reactor studies, verifying that there were no mass-transfer issues. In an effort to understand the mechanism behind the reaction, which has not been studied in water before, we performed surface-enhanced Raman spectroscopy (SERS) to observe the CF HDC reaction occur over a Pd-on-Au surface. By decorating Au nanoshells (NSs, a well-studied SERS substrate) with Pd atoms to emulate the Pd-on-Au NPs, we gained insights into how the CF HDC reaction initiates and proceeds to form methane.

Experimental Methods

Oxide-supported Pd/Au bimetallic catalyst preparation

Au/Al_2O_3 pellets (received from Mintek Johannesburg, South Africa; commercially available from Strem Chemicals, Newburyport, MA) were crushed and sieved into a powder with particle sizes smaller than 300 μm (US standard 50 mesh) (Figure 1). The powder was placed in a 50-mL glass vial containing 22 mL of a H_2PdCl_4 solution (2.4 mM, pH ~2.5) containing $PdCl_2(H_2O)_2$ as the predominant chemical species.[56] Adding the Au/Al_2O_3 powder to the solution increased the pH to ~6.5–8.0.

The Au/Al_2O_3 support amount (2.57, 1.29, 0.86 and 0.51 g) was chosen such that the final Pd weight loadings (0.02, 0.04, 0.06 and 0.10 wt %) were varied while the Pd content in the vial was constant (2.8×10^{-6} mol in 173-mL reaction fluid, or 0.017 g/L). Hydrogen gas was bubbled vigorously through the suspension for ~5 min to ensure good mixing, in a process similar to Pd-on-Au NP synthesis.[49,50] The catalyst suspension was dried afterwards overnight in a drying oven at 338 K. The resulting materials were designated as "$Pd/Au/Al_2O_3$". Detailed information about materials used and nitrogen physisorption characterization is provided online in Supporting Information.

Transmission Electron Microscopy. Transmission electron microscopy (TEM) images were collected using a JEOL 2010 transmission electron microscope operating at 100 kV. Au/Al_2O_3 supports and Pd/Al_2O_3 (~50 mg) were mixed with ~5 mL ethanol and stirred for 1 min. The supports were deposited onto 200-mesh carbon/Formvar grids by evaporating 1 drop of the sample suspension at room temperature. The number-average size distributions of 50+ particles were determined for each sample using ImageJ Software.

Chloroform hydrodechlorination reaction studies

CF HDC experiments were conducted in sealed batch reactors. All reactions were conducted at ambient conditions (296 K and 1 atm) at pH 7 under constant stirring. Headspace gas samples were withdrawn periodically and analyzed through gas chromatography (GC). Liquid-phase concentrations were estimated from the measured gas-phase concentrations of CF, dichloromethane (DCM), chloromethane (CM), and methane. Additional details are provided in Supporting Information.

Figure 1. Example of $Pd/Au/Al_2O_3$ prepared from Au/Al_2O_3 pellets (1.2 wt% Au).

[Color figure can be viewed in the online issue, which is available at wileyonlinelibrary.com.]

The reaction rate constants were approximated by assuming pseudo first-order rate dependence with respect to chloroform concentration

$$-\frac{dC_{CF}}{dt} = r_{\text{observed}} = k_{\text{observed}} C_{CF} \quad (1)$$

$$k_{\text{observed}} = k_{\text{cat}} C_{\text{cat}} \quad (2)$$

in which k_{observed} (min^{-1}) is the first-order reaction rate constant, k_{cat} ($\text{Lg}_{\text{Pd}}^{-1}\ \text{min}^{-1}$) is the Pd-normalized rate constant, and C_{cat} is the catalyst charge concentration (0.017 $\text{g}_{\text{Pd}}\text{L}^{-1}$). Carbon balance was calculated as the sum of unreacted CF (inside the reactor, which includes gas and liquid phase) and detected products (DCM, CM, and methane) divided by the initial CF amount. Selectivity values were calculated as total amount of a reaction product divided by the sum of DCM, CM, and methane products. All chromatograms were also analyzed for the presence of two-carbon compounds. All experiments were restricted to 60 min or less.

Surface-enhanced Raman spectroscopy (SERS)

Following the technique developed for analyzing dichloroethene hydrodechlorination under real-time, *in situ* conditions,[57] SERS was used to identify adsorbed surface intermediates during CF HDC using Pd-decorated gold nanoshell ("Pd-on-Au NSs") as a model for $Pd\text{-}Au/Al_2O_3$. The NSs were silica particles of 120 nm coated with a gold shell (2–3 nm thickness), further coated with Pd atoms at a calculated surface coverage of 60%. The method details are provided in Supporting Information.

Results and Discussion

Mass-transfer analysis

Several experiments were conducted to ensure proper consideration of mass-transfer effects on observed reaction rates. The k_{observed} values collected at different 1 wt% Pd/Al_2O_3 catalyst charges showed a linear relationship, indicating the collected reaction rate data method did not require correction for mass-transfer effects (Figure 2a). The slope of this line was 6.4 $\text{Lg}_{\text{Pd}}^{-1}\ \text{min}^{-1}$, equal to the rate constant calculated using Eq. 1 and 2 (Table 1), which indicated the rate determination procedure using one catalyst charge was correct. A similar analysis was conducted for $Pd/Au/Al_2O_3$ (0.04 wt% Pd and 1.2 wt% Au), which resulted in a straight line with slope of 22.0 $\text{Lg}_{\text{Pd}}^{-1}\ \text{min}^{-1}$, also equal to the rate constant calculated using Eqs. 1 and 2. The reciprocal plots were linear and its extrapolated y-intercept was zero, indicating the stirring rate was sufficiently high for negligible gas-liquid mass-transfer effect (Figure 2b).[58]

Catalyst structure

TEM analysis showed Au/Al_2O_3 with a 1.2 wt% Au loading to have NPs with an average size of 2.3 ± 0.8 nm (Figure 3a), within one standard deviation of the 2.8 ± 1.3 nm value reported by others.[59] Au/Al_2O_3 with a 0.9 wt% Au loading had an average size of 2.5 ± 0.7 nm (Figure S3). NPs Deposition of Pd appeared to increase negligibly the particle size (Figure 3b). For comparison, the Pd/Al_2O_3 material had an average particle size of 2.7 ± 1.1 nm. The Au/Al_2O_3 materials had larger BET surface areas (260 vs. 200 m^2/g) and smaller pore volumes and pore sizes than Pd/Al_2O_3 (Table S1).

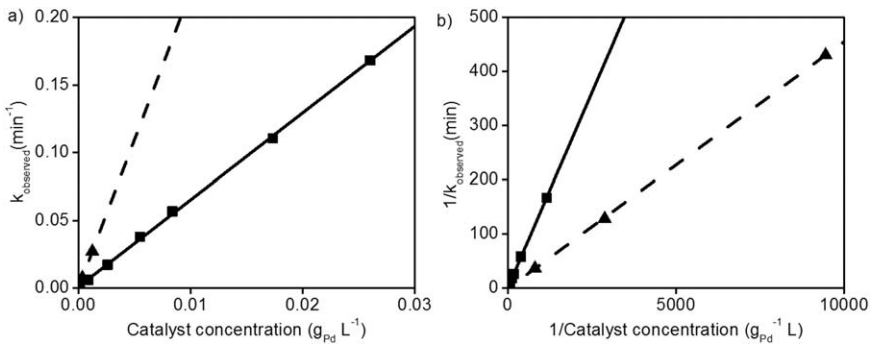

Figure 2. (a) Observed reaction rates (1/min) of 1 wt% Pd/Al_2O_3 (■, solid line) and $Pd/Au/Al_2O_3$ (0.04 wt% Pd, 1.2 wt% Au) (▲, dashed line) for CF HDC determined at different catalyst charge amounts (g_{Pd}/L); (b) the same results plotted as 1/(observed reaction rates) vs. 1/(catalyst concentration).

Table 1. First-Order Rate Constants (L g_{Pd}^{-1} min^{-1}) CF HDC Under Buffered Conditions

	Pd loading (wt%)					
Au loading (wt%)	0.00	0.02	0.04	0.06	0.10	1.0
0.0	—	—	—	—	—	6.4
0.9	0.0	17.9	12.5	9.7	12.8	—
1.2	0.0	15.0	22.4	13.5	21.1	—

The rate constants are the average of three reaction runs, with a relative standard deviation less than 10%. Reaction conditions: room temperature, 1 atm, pH 7, bicarbonate buffer solution. An example calculation is provided online in Supporting Information.

CF HDC Catalytic Activity. All materials containing Pd metal were catalytically active for CF HDC, and Au/Al_2O_3 materials at both Au loadings were inactive (Table 1 and Figure S1 online). $Pd/Au/Al_2O_3$ had higher rate constants than Pd/Al_2O_3, with the most active catalyst having a composition of 0.04 wt% Pd and 1.2 wt % Au. The pH of the reaction medium was maintained at 7 with the bicarbonate buffer (20 mL). Without the buffer, the pH rapidly decreased to ~4 due to proton generation ($CHCl_3 + 3H_2 = CH_4 + 3HCl$), resulting in a decrease of the catalytic activity (see online in Supporting Information for Figure S2). Based on our experience with Pd-on-Au NP synthesis (in which Pd^0 atoms deposited onto the Au NP surface during the H_2 bubbling step of the catalyst preparation method),[49,50] we presumed that some of the Pd^0 atoms formed via the reduction of $PdCl_2(H_2O)_2$ species also deposited on the Au surface.

We did not observe a clear dependence of catalytic activity on Pd content nor did we observe the volcano-shape activity dependence that Pd-on-Au NPs show.[52,53] The lack of a trend may be due to the presence of monometallic Pd domains and Au domains decorated with variable amounts of Pd. Nevertheless, the higher per-gram-Pd activities for the $Pd/Au/Al_2O_3$ samples (compared to Pd/Al_2O_3) strongly implied the presence of Pd-decorated Au domains.

We observed that the reaction rates increased when the Au loading increased from 0.9 wt % to 1.2 wt %, for all but the 0.02 wt % Pd case. The 1.2 wt % Au/Al_2O_3 material contained ~33% more Au than the 0.9 wt % material in terms of metal mass, volume, and (because the Au domains of both materials were essentially the same size) particle number. A simple scaling analysis (surface area $\propto$ mass$^{2/3}$) suggests the 1.2 wt % Au/Al_2O_3 has ~21% more surface area onto which Pd can deposit, leading to a lower coverage of the Au surface by Pd metal for a given Pd loading. That the higher Au-content samples were more active than the lower Au-content samples suggests the Pd atoms are more dispersed on the Au domains in the 1.2 wt % Au-containing materials.

CF HDC product distribution

All catalysts produced methane with >90% selectivity, calculated at a CF conversion of 32% (all catalysts showed a minimum of 32% conversion by end of reaction run). Carbon balances (accounting for measured gas- and liquid-phase concentrations of CF, DCM, CM, and methane) were reasonably close to 100%. Monometallic Pd/Al_2O_3 produced methane and DCM as products, with selectivities of 90 and 10%, respectively (Figure 4a). No CM was detected. The $Pd/Au/Al_2O_3$ materials produced methane, CM and DCM, with selectivities of 94.4%, 0.1% and 5.5%, respectively; Figure 4b shows the typical product concentration profiles. Nonzero CM concentrations were observed below 0.2 μmol/L, roughly the detection limit of our instrumentation. Trace amounts of ethane byproduct were also detected with all catalysts.

Spectroscopic observations of CF HDC surface reaction

To gain insights into how CF hydrodechlorinates over the $Pd/Au/Al_2O_3$ catalyst, we next studied the reaction spectroscopically using Pd-deposited Au NSs, a structure engineered to give strong SERS enhancement.[57,60] The noble nature of Au makes it an excellent SERS substrate, stemming to the small imaginary part of its dielectric function as compared to transition metals such as Pd. The Pd-on-Au NSs were prepared and immobilized onto a silicon substrate, which was then placed in a sealed, flow-through chamber for SERS analysis.

Initially, we analyzed the HDC reaction by adding dissolved CF and H_2 together in water to the analysis chamber. The baseline spectra changed and the Raman intensity increased significantly in the 200–300 cm^{-1} and 800–1600 cm^{-1} regions, but few peaks could be distinguished (Figure S4 online). Due to the rapidity of the reaction, we then carried out an experiment in which CF and H_2 were added separately. The SERS chamber was filled with water containing

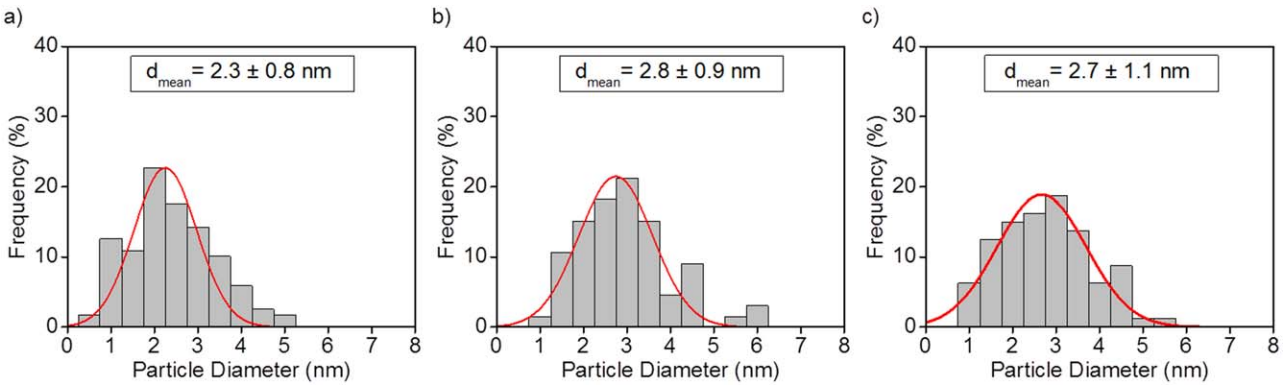

Figure 3. Size distribution of metal particles contained in (a) Au/Al2O3 (1.2 wt% Au), (b) $Pd/Au/Al_2O_3$ (0.04 wt% Pd, 1.2 wt% Au), and (c) 1 wt% Pd/Al_2O_3.

Each bar represents the fraction of NPs with a diameter within ±0.25 nm. [Color figure can be viewed in the online issue, which is available at wileyonlinelibrary.com.]

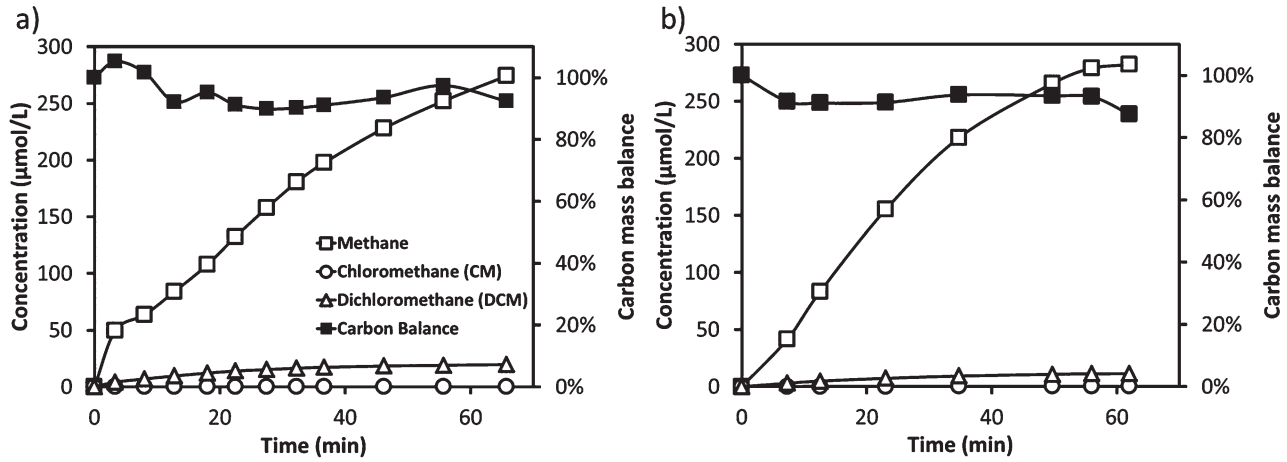

Figure 4. Headspace concentration-time and carbon balance profiles for CF HDC using (a) Pd/Al_2O_3 (1 wt% Pd) and (b) $Pd/Au/Al_2O_3$ (0.10 wt% Pd, 1.2 wt% Au).

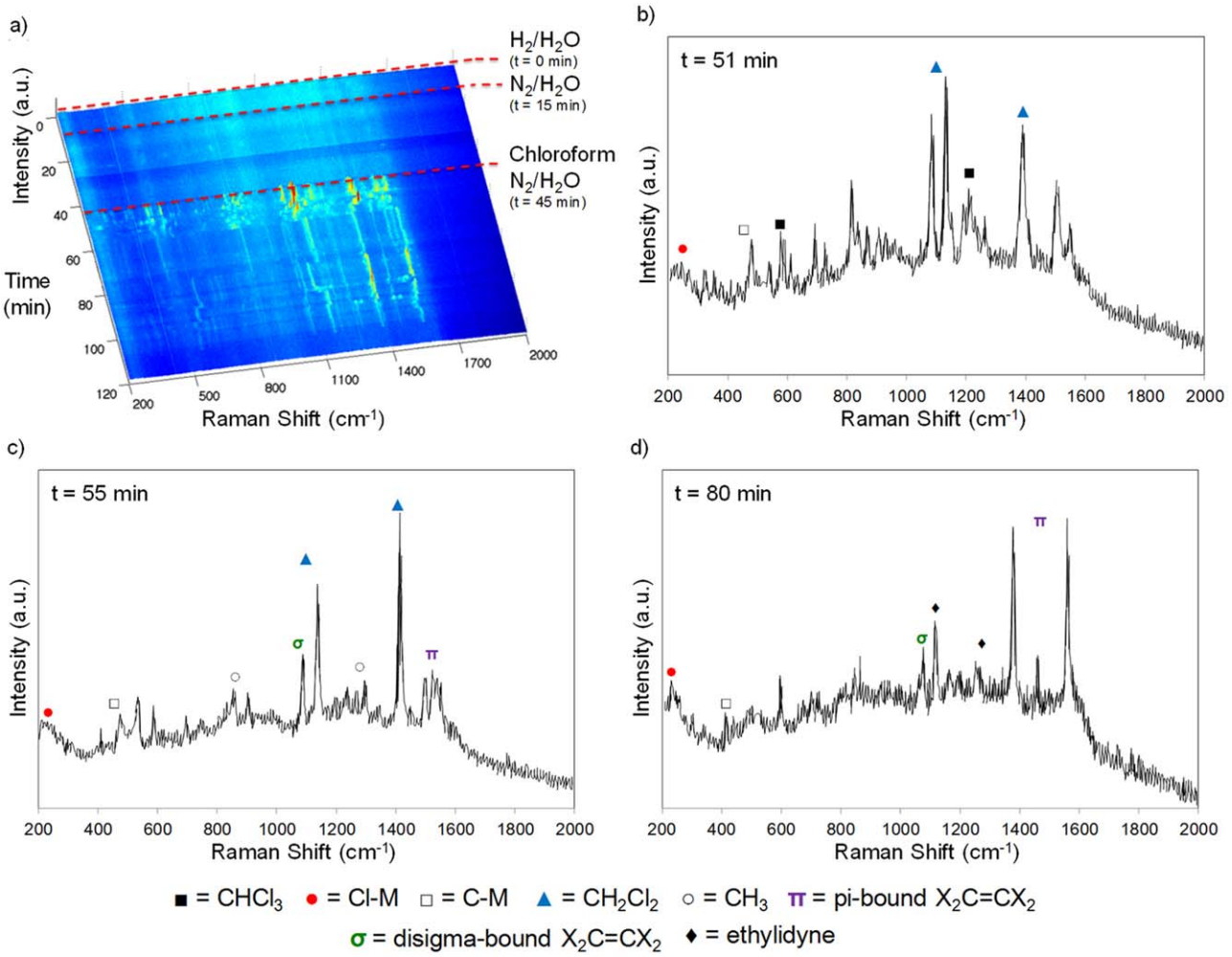

Figure 5. (a) Surface-enhanced Raman spectra collected (a) over a period of 2 hr, (b) at 51 min, (c) at 55 min, and (d) at 80 min.

SERS conditions: Pd-on-Au NSs immobilized on silicon, room temperature, liquid-phase CF concentration = 0.503 mM (60 ppm). CF-containing water was introduced at t = 45 min, after H2- and N2-containing water was introduced at t = 0 and 15 min, respectively. [Color figure can be viewed in the online issue, which is available at wileyonlinelibrary.com.]

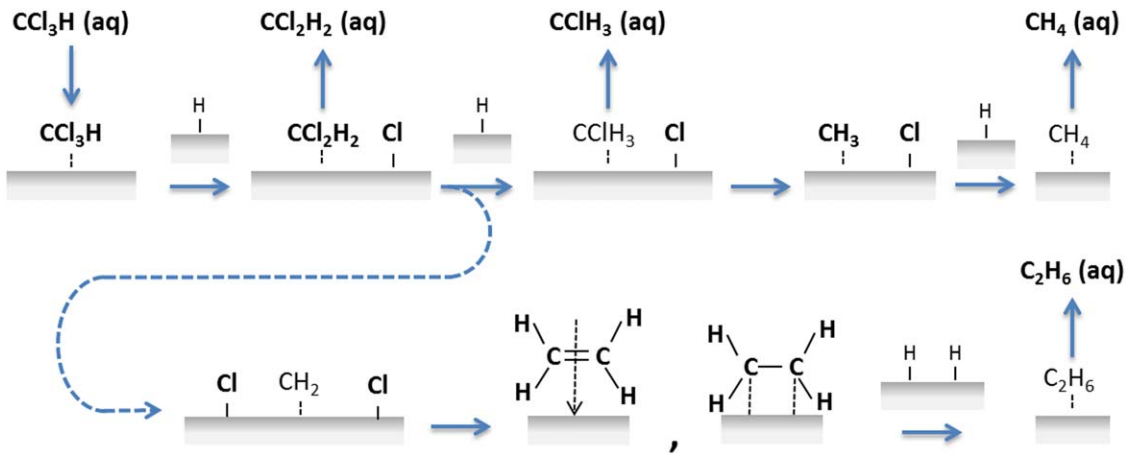

Scheme 1. Proposed CF HDC reaction pathway to methane.

The detected chemical species (from SERS using Pd-on-Au NSs and batch reactor studies using Pd/Au/Al_2O_3) are shown in bold. The dashed arrow shows the minor pathway to ethane.

H_2 and sealed at $t = 0$ min and then repeated with water containing N_2 at $t = 15$ min to flush away any H_2 remaining in solution. No spectral features appeared under either condition (Figure 5a). After CF-containing water was introduced and the chamber was sealed, sharp Raman features emerged.

In comparison, no peaks appeared when CF-containing water was introduced into the chamber without the H_2 passing through first (Figure S4). These observations suggested that some H_2 remained on the Pd surface (as H atoms from the dissociative adsorption of H_2) after it was swept out of the chamber, and that these species were important to causing CF to react.

There have been spectroscopic studies focusing on the adsorption of halogenated methanes on single crystal surfaces, but none have focused on the transformation of CF in water.[61,62] At $t = 51$ min, a possible adsorbed CF molecule was detected with a stretching mode of C—Cl_3 at 690 cm^{-1} and a CH bend at 1210 cm^{-1}, close to the gas phase values of 760 and 1217 cm^{-1} of free CF.[63] Dechlorination and chemisorption of the C atom to the surface of the the catalyst was apparent, with a broad band for Cl-metal bonding in the 200–300 cm^{-1} range,[64] and a broad C-metal peak near ~400 cm^{-1}. There is some evidence of these species reacting with H atoms chemisorbed to the surface; peaks at ~1100 cm^{-1} and ~1400 cm^{-1} could be due to C—Cl_2 torsion and C—H_2 scissor modes of dichloromethane, respectively.[63] In addition to being the hydrogen and electron donor for the CF HDC reaction, H_2 (in the form of surface H atoms) appeared to initiate the dechlorination of adsorbed CF.[65]

At $t = 55$ min, hydrogenated species were found with bands at 857 and 1300 for C—H vibrational modes and 1416 cm^{-1} for CH_3 deformation.[63] Bands at ~1500 cm^{-1} and ~1100 cm^{-1} appeared and grew, which were similar to characteristic modes of pi- and di-sigma- bound ethylene, respectively.[66] These bands are evidence of coupling between carbon atoms which occur under the low-hydrogen content compared to the bulk experiment, as observed previously in our dichloroethene hydrodechlorination SERS study.[57] Ethane was detected in trace amounts in our CF HDC reactor studies, as noted before. At the end of the experiment ($t = 80$ min), almost all modes that could be associated with C—Cl stretching disappeared, perhaps indicative of complete dechlorination of the CF. The peaks ~1500 and ~1100 cm^{-1}, and a new peak at ~1300 cm^{-1}, and the C—C stretching band at ~1100 cm^{-1} suggested the umbrella mode of ethylidyne.[66] Based on our spectroscopic findings and batch reactor results, we propose that CF dechlorinates into methane through a sequence of surface reaction steps, forming very small amounts of DCM, CM and ethane (Scheme 1).

Conclusions

Supported Pd catalysts are active for the degradation of CF in water at room temperature and atmospheric pressure. The presence of hydrogen gas is necessary as the reducing agent for this catalytic reaction, which converts CF into near quantitative amounts of methane. Rigorous kinetics analysis properly assess and account for mass transfer effects on observed kinetic rates. Pd/Al_2O_3 containing 1 wt% Pd was active ($k_{cat} = 6.7$ Lg_{Pd}^{-1} min^{-1}), although quite slow compared to HDC reactions of other chlorinated contaminants. The reaction rate is increased by the presence of Au metal, in the form of Pd/Au/Al_2O_3 prepared by depositing Pd metal onto commercially available Au/Al_2O_3. A library of Pd/Au/Al_2O_3 samples containing different amounts of Pd and Au metals revealed that all bimetallic catalysts were more active, with the most active one containing 0.04 wt % Pd and 1.2 wt % Au ($k_{cat} = 22.4$ Lg_{Pd}^{-1} min^{-1}). Further work to assess the Pd-on-Au nanostructure in Pd/Au/Al_2O_3 and to improve the synthesis method is needed. Through *in aquo* surface-enhanced Raman spectroscopy, the CF HDC reaction appears to start with the chemisorption of chloroform, which occurs only in the presence of H_2. Detection of surface intermediates are consistent with the stepwise dechlorination of CF into methane and coupled species. These findings point to the usefulness of Au as a promoting metal in water-phase catalytic reactions, especially in water clean-up applications.

Acknowledgments

This work is supported by the Welch Foundation (C-1676), the National Science Foundation (CBET-1134535, DGE-0504425, EEC-0647452), SABIC Americas, World Gold Council, and Rice University. We gratefully acknowledge the Alliance for Graduate Education and Professoriate (AGEP) for providing additional support. We thank Dr. D. Ramdayal and Dr. J. McPherson (Mintek, South Africa) for kindly providing the Au/Al_2O_3 support materials and for useful discussions, and DCG Partnership for providing the calibration gas mixture. We thank Ms. L Pretzer and Dr. G. C. Kini for the TEM images. Finally, we acknowledge Mr. B. S. Nave (DuPont) and Dr. J. A. Wilkens (DuPont) for very helpful discussions, and Dr. J. H. Hafner (Rice) for plasma cleaner usage.

Literature Cited

1. Zogorski J, Carter J, Ivahnenko T, et al. The Quality of our Nation's Waters-Volatile Organic Compounds in the Nation's Ground Water and Drinking-Water Supply Wells. US Geological Survey Circular; 2006;1292:101.
2. ATSDR 2011 Substance Priority List. 2011. http://www.atsdr.cdc.gov/SPL/resources/index.html. Accessed January 24, 2011.
3. Toxicological profile for Chloroform. Atlanta, GA: US. Dept of Health and Human Services, Public Health Service; 1997.
4. EPA US. Toxicological review of chloroform (CAS No. 67-66-3) : In support of summary information on the integrated risk information system (IRIS) 2001; http://www.epa.gov/IRIS/. Available at: http://www.epa.gov/iris/toxreviews/0025-tr.pdf.
5. EPA US. National Primary Drinking Water Regulations: Disinfectants and Disinfection Byproducts; Final Rule, Environmental Protection Agency; 1998.
6. Gaube J, Boublik T, Fried V, Hala E. The vapour pressures of pure substances-Selected values of the temperature dependence of the vapour pressures of some pure substances in the normal and low pressure region (revised 2nd ed). Berichte der bunsengesellschaft für physikalische chemie, 1985;89(3):352–352.
7. Eisenreich SJ, Looney BB, Thornton JD. Airborne organic contaminants in the Great Lakes ecosystem. *Environ Sci Technol*. 1981;15(1):30–38.
8. Gossett JM. Measurement of Henry's law constants for C1 and C2 chlorinated hydrocarbons. *Environ Sci Technol*. 1987;21(2):202–208.
9. Jeffers PM, Ward LM, Woytowitch LM, Wolfe NL. Homogeneous hydrolysis rate constants for selected chlorinated methanes, ethanes, ethenes, and propanes. *Environ Sci Technol*. 1989;23(8):965–969.
10. Hampson RF. *Chemical Kinetic and Photochemical Data Sheets for Atmospheric Reactions*. DOT-FA79WAI-005, Document ID: 19810006027.: National Aeronautics and Space Administration; 1980:489.
11. Singh HB, Salas LJ, Smith AJ, Shioeishi H. Measurements of some potentially hazardous organic chemicals in urban environments. *Atmos Environ (1967)*. 1981;15(4):601–612.
12. Atkinson R. Kinetics and mechanisms of the gas-phase reactions of the hydroxyl radical with organic compounds under atmospheric conditions. *Chem Rev*. 1986;86(1):69–201.
13. Clark CS, Meyer CR, Gartside PS, et al. An environmental health survey of drinking water contamination by leachate from a pesticide waste dump in hardeman county, tennessee. *Arch Environ Health*. 1982;37(1):9.
14. Sabljic A. Predictions of the nature and strength of soil sorption of organic pollutants by molecular topology. *J Agric Food Chem*. 1984;32(2):243–246.
15. Soil vapor extraction (SVE) at six drycleaner sites. http://costperformance.org/profile.cfm?ID = 345&CaseID = 345. Accessed January 24, 2011.
16. Soil vapor extraction at the sand creek industrial superfund site, operable unit No. 1. http://costperformance.org/profile.cfm?ID = 242&CaseID = 242. Accessed January 11, 2011.
17. Thermal desorption at the rocky flats environmental technology site, trenches T-3 and T-4. http://costperformance.org/profile.cfm?ID = 235&CaseID = 235. Accessed August 4, 2011.
18. Pump and treat and containment of contaminated groundwater at the sylvester/gilson road superfund site. 1981; http://costperformance.org/profile.cfm?ID = 276&CaseID = 276. Accessed August 12, 2011.
19. Pump and treat of contaminated groundwater at the ott/story/cordova superfund site, North Muskegon, Michigan. http://costperformance.org/profile.cfm?ID = 208&CaseID = 208. Accessed August 8, 2011.
20. Pump and treat of contaminated groundwater at the scrdi dixiana superfund site, Cayce, South Carolina. http://costperformance.org/profile.cfm?ID = 255&CaseID = 255. Accessed January 12, 2011.
21. Deployment of Phytotechnology in the 317/319 Area at Argonne National Laboratory-East. http://costperformance.org/profile.cfm?ID = 390&CaseID = 390. Accessed January 22, 2011.
22. Permeable reactive barriers (PRBs) interim summary report: prbs using injection and other emerging technologies. http://costperformance.org/profile.cfm?ID = 170&CaseID = 170. Accessed February 12, 2011.
23. Cap at DOE's Lawrence Livermore National Laboratory, Site 300, Pit 6 Landfill OU. http://costperformance.org/profile.cfm?ID = 131&CaseID = 131. Accessed January 21, 2011. Accessed March 13, 2011.
24. Natural attenuation of chlorinated volatile organic compounds in a freshwater tidal wetland, Aberdeen proving ground, Maryland. U.S. GEOLOGICAL SURVEY, Water-Resources Investigations Report 97-4171.
25. Pump and treat and in situ bioremediation of contaminated groundwater at the French, Ltd. Superfund Site, Crosby, TX. Available at: http://costperformance.org/pdf/French%20Limited.pdf. Accessed January 24, 2011.
26. Chen N, Rioux R, Barbosa L, Ribeiro F. Kinetic and theoretical study of the hydrodechlorination of CH4-xClx (x = 1–4) compounds on palladium. *Langmuir*. 2009;26(21):16615–16624.
27. Dal Santo V, Dossi C, Recchia S, Colavita PE, Vlaic G, Psaro R. Carbon tetrachloride hydrodechlorination with organometallics-based platinum and palladium catalysts on MgO. *J Mol Catal A Chem*. 2002;182-183(0):157–166.
28. Musialik-Piotrowska A. Destruction of trichloroethylene (TCE) and trichloromethane (TCM) in the presence of selected VOCs over Pt-Pd-based catalyst. *Catal Today*. 2007;119(1-4):301–304.

29. Noelke CJ, Rase HF. Improved hydrodechlorination catalysis: chloroform over platinum-alumina with special treatments. *Ind Eng Chem Prod Res Develop*. 1979/12/01 1979;18(4):325–328.
30. CERCLA Priority List of Hazardous Substances, Agency for Toxic Substances and Disease Registry-US Dept of Health and Human Services; 2007.
31. Matheson LJ, Tratnyek PG. Reductive dehalogenation of chlorinated methanes by iron metal. *Environ Sci Technol*. 1994;28(12):2045–2053.
32. Hsiao C, Lee C, Ollis D. Heterogeneous photocatalysis: Degradation of dilute solutions of dichloromethane (CH2Cl2), chloroform (CHCl3), and carbon tetrachloride (CCl4) with illuminated TiO2 photocatalyst. *J Catal*. 1983;82(2):418–423.
33. Pruden AL, Ollis DF. Degradation of chloroform by photoassisted heterogeneous catalysis in dilute aqueous suspensions of titanium dioxide. *Environ Sci Technol*. 1983;17(10):628–631.
34. Weathers LJ, Parkin GF, Alvarez PJJ. Utilization of cathodic hydrogen as electron donor for chloroform cometabolism by a mixed, methanogenic culture. *Environ Sci Technol*. 1997;31(3):880–885.
35. Wang X, Chen C, Chang Y, Liu H. Dechlorination of chlorinated methanes by Pd/Fe bimetallic nanoparticles. *J Hazard Mater*. 2009;161(2-3):815–823.
36. Muftikian R, Fernando Q, Korte N. A method for the rapid dechlorination of low-molecular-weight chlorinated hydrocarbons in water. *Water Res*. 1995;29(10):2434–2439.
37. Zhang W, Wang C, Lien H-L. Treatment of chlorinated organic contaminants with nanoscale bimetallic particles. *Catal Today*. 1998;40(4):387–395.
38. Alonso F, Beletskaya IP, Yus M. Metal-mediated reductive hydrodehalogenation of organic halides. *Chem Rev*. 2002;102(11):4009–4092.
39. Urbano FJ, Marinas JM. Hydrogenolysis of organohalogen compounds over palladium supported catalysts. *J Mol Catal A Chem*. 2001;173(1-2):329–345.
40. Lien H-L, Zhang W-x. Nanoscale iron particles for complete reduction of chlorinated ethenes. *Colloids Surfaces A*. 2001;191(1-2):97–105.
41. McNab WW, Ruiz R. Palladium-catalyzed reductive dehalogenation of dissolved chlorinated aliphatics using electrolytically-generated hydrogen. *Chemosphere*. 1998;37(5):925–936.
42. Wang C-B, Zhang W-x. Synthesizing nanoscale iron particles for rapid and complete dechlorination of TCE and PCBs. *Environ Sci Technol*. 1997;31(7):2154–2156.
43. Schreier CG, Reinhard M. Catalytic hydrodehalogenation of chlorinated ethylenes using palladium and hydrogen for the treatment of contaminated water. *Chemosphere*. 1995;31(6):3475–3487.
44. Schüth C, Reinhard M. Hydrodechlorination and hydrogenation of aromatic compounds over palladium on alumina in hydrogen-saturated water. *Applied Catalysis B*. 1998;18(3-4):215–221.
45. Lowry GV, Reinhard M. Hydrodehalogenation of 1- to 3-carbon halogenated organic compounds in water using a palladium catalyst and hydrogen gas. *Environ Sci Technol*. 1999;33(11):1905–1910.
46. Lowry GV, Reinhard M. Pd-catalyzed TCE dechlorination in groundwater: Solute effects, biological control, and oxidative catalyst regeneration. *Environ Sci Technol*. 2000;34(15):3217–3223.
47. Lowry GV, Reinhard M. Pd-catalyzed TCE dechlorination in water: Effect of [H2](aq) and H2-utilizing competitive solutes on the TCE dechlorination rate and product distribution. *Environ Sci Technol*. 2001;35(4):696–702.
48. Schüth C, Disser S, Schüth F, Reinhard M. Tailoring catalysts for hydrodechlorinating chlorinated hydrocarbon contaminants in groundwater. *Appl Catal B*. 2000;28(3-4):147–152.
49. Nutt MO, Hughes JB, Wong MS. Designing Pd-on-Au bimetallic nanoparticle catalysts for trichloroethene hydrodechlorination. *Environ Sci Technol*. 2005;39(5):1346–1353.
50. Nutt MO, Heck KN, Alvarez PJJ, Wong MS. Improved Pd-on-Au bimetallic nanoparticle catalysts for aqueous-phase trichloroethene hydrodechlorination. *Appl Catalysis B*. 2006;69(1-2):115–125.
51. Heck KN,Nutt MO, Alvarez PJJ, Wong MS. Deactivation resistance of Pd/Au nanoparticle catalysts for water-phase hydrodechlorination. *J Catal*. 2009;267(2):97–104.
52. Pretzer LA, Song HJ, Fang Y-L, et al. Hydrodechlorination catalysis of Pd-on-Au nanoparticles varies with particle size. *J Catal*. 2013;298(0):206–217.
53. Zhao Z, Fang Y-L, Alvarez PJJ, Wong MS. Degrading perchloroethene at ambient conditions using Pd and Pd-on-Au reduction catalysts. *Appl Catal B*. 8//2013;140-141(0):468–477.
54. Wong MS, Alvarez PJJ, Fang YL, et al. Cleaner water using bimetallic nanoparticle catalysts. *J Chem Technol Biot*. 2009;84(2):158–166.
55. Davie MG, Cheng H, Hopkins GD, LeBron CA, Reinhard M. Implementing heterogeneous catalytic dechlorination technology for remediating tce-contaminated groundwater. *Environ Sci Technol*. 2008;42(23):8908–8915.
56. Elding LI. Palladium(II) halide complexes. I. Stabilities and spectra of palladium(II) chloro and bromo aqua complexes. *Inorg Chimi Acta*. 1972;6(0):647–651.
57. Heck KN, Janesko BG, Scuseria GE, Halas NJ, Wong MS. Observing metal-catalyzed chemical reactions in situ using surface-enhanced Raman spectroscopy on Pd−Au nanoshells. *J Am Che Soc*. 2008;130(49):16592–16600.
58. Fang Y-L, Heck KN, Alvarez PJJ, Wong MS. Kinetics analysis of palladium/gold nanoparticles as colloidal hydrodechlorination catalysts. *ACS Catal*. 2011;1(2):128–138.
59. Walther G, Cervera-Gontard L, Quaade U, Horch S. Low temperature methane oxidation on differently supported 2 nm Au nanoparticles. *Gold Bulletin*. 2009;42(1):13–19.
60. Jackson JB, Westcott SL, Hirsch LR, West JL, Halas NJ. Controlling the surface enhanced Raman effect via the nanoshell geometry. *Appl Phys Lett*. 2003;82(2):257–259.
61. Bent BE. Mimicking aspects of heterogeneous catalysis: Generating, isolating, and reacting proposed surface

intermediates on single crystals in vacuum. *Chem Rev*. 1996;96(4):1361–1390.
62. Chesters MA, Lennon D. The adsorption of carbon tetrachloride on Ni(110): an EELS, AES and LEED study. *Surface Sci*. 1999;426(1):92–105.
63. Shimanouchi T. *Tables of Molecular Vibrational Frequencies Consolidated* Vol I, National Bureau of Standards; 1972;1–160. 1972.
64. Clark RJH, Michael DJ. Resonance Raman spectra of metal II/IV dimer chain complexes of platinum and palladium: Analysis of the component structure to the band assigned to the symmetric XMX chain stretching mode (X = Cl or Br). *J Mol Structure*. 1988;189(1-2): 173–185.
65. Gomez-Sainero LM, Seoane XL, Tijero E, Arcoya A. Hydrodechlorination of carbon tetrachloride to chloroform in the liquid phase with a Pd/carbon catalyst. Study of the mass transfer steps. *Chem Eng Sci*. 2002;57(17):3565–3574.
66. Sheppard BH, Jon H, Warshaw PR. The theory of reasoned action: a meta-analysis of past research with recommendations for modifications and future research. *J Consume Res*. 1988;15(3):325–343.

Manuscript received Sept. 12, 2013, revision received July 17, 2013, and final revision received Sept. 29, 2013.